The Plant Cell, Vol. 23: 2774–2787, July 2011, www.plantcell.org

Symbiotic Rhizobia Bacteria Trigger a Change in Localization and Dynamics of the *Medicago truncatula* Receptor Kinase LYK3 [W] [OA]

Cara H. Haney,[a] Brendan K. Riely,[b] David M. Tricoli,[b,c] Doug R. Cook,[b] David W. Ehrhardt,[a,d] and Sharon R. Long[a,1]

[a] Department of Biology, Stanford University, Stanford, California 94305
[b] Department of Plant Pathology, University of California, Davis, California 95616
[c] The Ralph M. Parsons Foundation Plant Transformation Facility, University of California, Davis, California 95616
[d] Department of Plant Biology, Carnegie Institution for Science, Stanford, California 94305

To form nitrogen-fixing symbioses, legume plants recognize a bacterial signal, Nod Factor (NF). The legume *Medicago truncatula* has two predicted NF receptors that direct separate downstream responses to its symbiont *Sinorhizobium meliloti*. *NOD FACTOR PERCEPTION* encodes a putative low-stringency receptor that is responsible for calcium spiking and transcriptional responses. *LYSIN MOTIF RECEPTOR-LIKE KINASE3* (*LYK3*) encodes a putative high-stringency receptor that mediates bacterial infection. We localized green fluorescent protein (GFP)-tagged LYK3 in *M. truncatula* and found that it has a punctate distribution at the cell periphery consistent with a plasma membrane or membrane-tethered vesicle localization. In buffer-treated control roots, LYK3:GFP puncta are dynamic. After inoculation with compatible *S. meliloti*, LYK3:GFP puncta are relatively stable. We show that increased LYK3:GFP stability depends on bacterial NF and NF structure but that NF is not sufficient for the change in LYK3:GFP dynamics. In uninoculated root hairs, LYK3:GFP has little codistribution with mCherry-tagged FLOTILLIN4 (FLOT4), another punctate plasma membrane–associated protein required for infection. In inoculated root hairs, we observed an increase in FLOT4:mCherry and LYK3:GFP colocalization; both proteins localize to positionally stable puncta. We also demonstrate that the localization of tagged FLOT4 is altered in plants carrying a mutation that inactivates the kinase domain of *LYK3*. Our work indicates that LYK3 protein localization and dynamics are altered in response to symbiotic bacteria.

INTRODUCTION

Plants in the family *Fabaceae* (legumes) form symbiotic relationships with nitrogen-fixing rhizobial bacteria. The bacteria live in association with plant roots inside morphologically unique structures called nodules. In this mutualistic interaction, the bacteria reduce (or fix) molecular dinitrogen to ammonia, a form of nitrogen that plants can use; in exchange, the plants supply the bacteria with carbon sources. Through this intimate metabolic partnership, both plant and bacteria benefit.

An exchange of signals initiates symbiosis between legumes and bacteria. Plant roots secrete flavonoids, which cause induction of bacterial genes required for synthesis of a lipochitooligosaccharide called Nod Factor (NF) (Fisher and Long, 1992). Within minutes of application of bacteria or purified NF, root hair membrane depolarization occurs (Ehrhardt et al., 1992). Within the first hour after NF treatment, cellular calcium levels begin to oscillate in root hairs and root epidermal cells (called calcium spiking) (Ehrhardt et al., 1996). A number of phenotypic changes occur in root hairs following calcium spiking. First, actively elongating root hairs stop growing and swell. The root hairs then reinitiate tip growth and grow to form a curl around a bacterial colony. Bacteria enter root hairs through plant-derived intracellular structures called infection threads. These events coincide with transcriptional changes that are largely NF dependent (Mitra et al., 2004a). Purified NF is sufficient to induce plant morphological and transcriptional changes but is not sufficient for infection thread formation.

The structure and biosynthesis of NF have been characterized in the model symbiotic bacterium *Sinorhizobium meliloti*. The NF backbone is a tetramer of β-1,4-linked *N*-acetyl glucosamine (Roche et al., 1991a). Modified forms of *S. meliloti* NF alter host specificity and elicit altered host responses. *NodH* mutants lack a C6-sulfate modification on the reducing residue and elicit no measurable plant response, including Ca^{2+} spiking (Roche et al., 1991b; Ehrhardt et al., 1995; Schultze et al., 1995; Wais et al., 2002). A *nodF* mutant produces a NF with a modified *N*-acylation on the terminal nonreducing *N*-acetyl glucosamine residue (Shearman et al., 1986; Demont et al., 1993). NF produced by *nodL* mutants lacks a C6-*O*-acetylation on the terminal nonreducing glucosamine (Ardourel et al., 1995). *NodFL* double mutants trigger Ca^{2+} spiking and root hair deformation but are unable to infect their hosts (Ardourel et al., 1994; Wais et al., 2002). The observation that altering NF structure either abolishes all plant responses or specifically abolishes infection led to a two-receptor model in host NF perception where (1) a less

[1] Address correspondence to srl@stanford.edu.
The author responsible for distribution of materials integral to the findings presented in this article in accordance with the policy described in the Instructions for Authors (www.plantcell.org) is: Doug R. Cook (drcook@ucdavis.edu).
[W] Online version contains Web-only data.
[OA] Open Access articles can be viewed online without a subscription.
www.plantcell.org/cgi/doi/10.1105/tpc.111.086389

stringent signaling receptor mediates calcium spiking and transcription and (2) a highly stringent entry receptor mediates bacterial entry into root hairs (Ardourel et al., 1994).

The two-receptor model is supported by genetic studies in *S. meliloti*'s host legume *Medicago truncatula*, which have identified two putative NF receptor loci, *NOD FACTOR PERCEPTION* (*NFP*) and *LYSIN MOTIF RECEPTOR-LIKE KINASE3* (*LYK3*). Both genes encode predicted *trans*-membrane receptors containing lysin motifs (LysM) (Limpens et al., 2003; Arrighi et al., 2006). LysM domains confer chitin binding activity to the *Arabidopsis thaliana* and rice (*Oryza sativa*) receptors *CHITIN ELICITOR RECEPTOR KINASE1* and *CHITIN ELICITOR BINDING PROTEIN* (Kaku et al., 2006; Iizasa et al., 2010; Petutschnig et al., 2010). As such, *M. truncatula* LYK3 and NFP are good candidates for binding the chitin backbone of NF. *NFP* mutants are completely insensitive to NF (Wais et al., 2002; Amor et al., 2003). By contrast, in response to *S. meliloti* and NF, *LYK3* mutants (also called *hair curling* [*hcl*]) undergo extensive root hair deformation and limited cortical cell divisions but do not form root hair curls or infection threads (Catoira et al., 2001; Limpens et al., 2003; Smit et al., 2007). Weaker mutant alleles of *lyk3*, and *LYK3* RNA interference plants, form infection threads that fail to penetrate the root cortex (Limpens et al., 2003; Smit et al., 2007). Based on these observations, *NFP* is proposed to encode the low-stringency receptor required for calcium spiking and gene expression, and *LYK3* is thought to encode the high-stringency receptor required for bacterial entry into root hairs (Limpens et al., 2003; Smit et al., 2007).

The *DOES NOT MAKE INFECTIONS* (*DMI*) signaling pathway functions genetically downstream of *NFP* and is also required for mycorrhizal symbiosis (Catoira et al., 2000). Studies in other model legumes, including *Lotus japonicus* and pea (*Pisum sativum*), have identified genes with homology and conserved function to *NFP*, *DMI*s, and others discussed below (reviewed in Oldroyd and Downie, 2008; Murray, 2011). The *DMI* pathway includes *DMI2*, a receptor-like kinase necessary for calcium spiking (Endre et al., 2002), a putative nuclear ion channel *DMI1* (Ané et al., 2004; Riely et al., 2007), and a calcium/calmodulin-dependent protein kinase encoded by *DMI3* (Levy et al., 2004; Mitra et al., 2004b). NODULATION SIGNALING PATHWAY transcription factors NSP1 and NSP2 are genetically downstream of the DMI pathway (Catoira et al., 2000; Oldroyd and Long, 2003). *NSP1,2* and the *DMI* pathway genes are dispensable for NF-induced membrane depolarization and root hair swelling but necessary for all NF-dependent transcriptional changes, nodule formation, and infection (Catoira et al., 2000; Mitra et al., 2004a).

LYK3 mutants are defective in infection but lack only a subset of NF-dependent transcriptional changes (Mitra et al., 2004a). How LYK3 influences infection is not as well understood as NFP-dependent signaling events. Genes required for infection are potential components of the LYK3 infection pathway. The E3-ubiquitin ligase PLANT U-BOX PROTEIN 1 (PUB1) interacts with LYK3 and negatively regulates infection. LYK3 may activate PUB1, which in turn ubiquitinates and consequentially promotes degradation of components of the infection pathway, or PUB1 may directly target LYK3 for degradation (Mbengue et al., 2010). A plant-specific gene, *RHIZOBIUM-DIRECTED POLAR GROWTH* (*RPG*), encodes a nuclear-localized protein with a long coiled-coil domain and is required for infection thread polar growth (Arrighi et al., 2008). Infection thread growth requires *REQUIRED FOR INFECTION THREADS* (*RIT1*), which is involved in actin reorganization (Miyahara et al., 2010). A membrane-associated flotillin *FLOT4* is required for infection thread elongation, as is a plant-specific remorin (Haney and Long, 2010; Lefebvre et al., 2010). These genes and others are known to be required for normal infection, but how they work cooperatively and integrate signals from the LYK3-dependent NF perception pathway remains to be determined.

The phenotype of the *M. truncatula* symbiotic mutant *nodule inception* (*nin*) suggests that crosstalk between NFP/DMI and LYK3 signaling pathways coordinates infection with nodule development. *NIN* encodes a putative transcriptional regulator and is required for nodule organogenesis and infection events but not for NF-dependent transcriptional changes (Marsh et al., 2007). NSP1 directly binds to the *NIN* promoter and is required for *NIN* expression (Hirsch et al., 2009). Elucidating the mechanisms by which *NIN* and other genes mechanistically enable crosstalk between nodule formation and infection pathways are a focus of ongoing work.

To gain insight into the cell biology of early events during host perception of a symbiotic bacterium, we localized a functional, green fluorescent protein (GFP)-tagged version of the *M. truncatula* symbiotic LysM receptor-kinase, LYK3. We monitored LYK3:GFP localization and behavior in uninoculated and *S. meliloti*–inoculated roots and characterized the dependence of protein behavior on NF structure. Our data suggest that NF-dependent changes in LYK3:GFP localization and dynamics may be important for regulating symbiotic infection.

RESULTS

LYK3:GFP Has a Punctate Distribution Associated with the Plasma Membrane

To localize the LYK3 protein, plants containing the LYK3 kinase-inactive mutant allele *hcl-1* (Klaus-Heisen et al., 2011) were stably transformed with a full genomic copy of *LYK3* (*pLYK3*:*gLYK3*) translationally fused to either *GFP* or a *HASt* dual-affinity tag. Root hair walls and other structures are known to display autofluorescence; the *HASt*-tagged lines were used as controls to distinguish the GFP signal from autofluorescence. We recovered two transgenic lines with each construct that formed nitrogen-fixing nodules (Figures 1A and 1B; Turner and Gibson, 1980). We also introduced *pLYK3*:*gLYK3*:*GFP* and *pLYK3*:*gLYK3*:*HASt* into the *LYK3* mutant *hcl-2* using *Agrobacterium rhizogenes*–mediated hairy root transformation and found that both constructs restored nodulation (see Supplemental Table 1 online). Pros and cons of hairy roots and stable transgenic plants in the study of symbiosis are discussed elsewhere (Boisson-Dernier et al., 2001; Crane et al., 2006).

In uninoculated root hairs, both in stable transgenic plants and in hairy roots transformed with *pLYK3*:*gLYK3*:*GFP*, we observed LYK3:GFP in a punctate distribution at the extreme cell periphery in a gradient that was denser near the growing tip (Figures 1C; see Supplemental Figure 1 online). The LYK3:GFP signal is

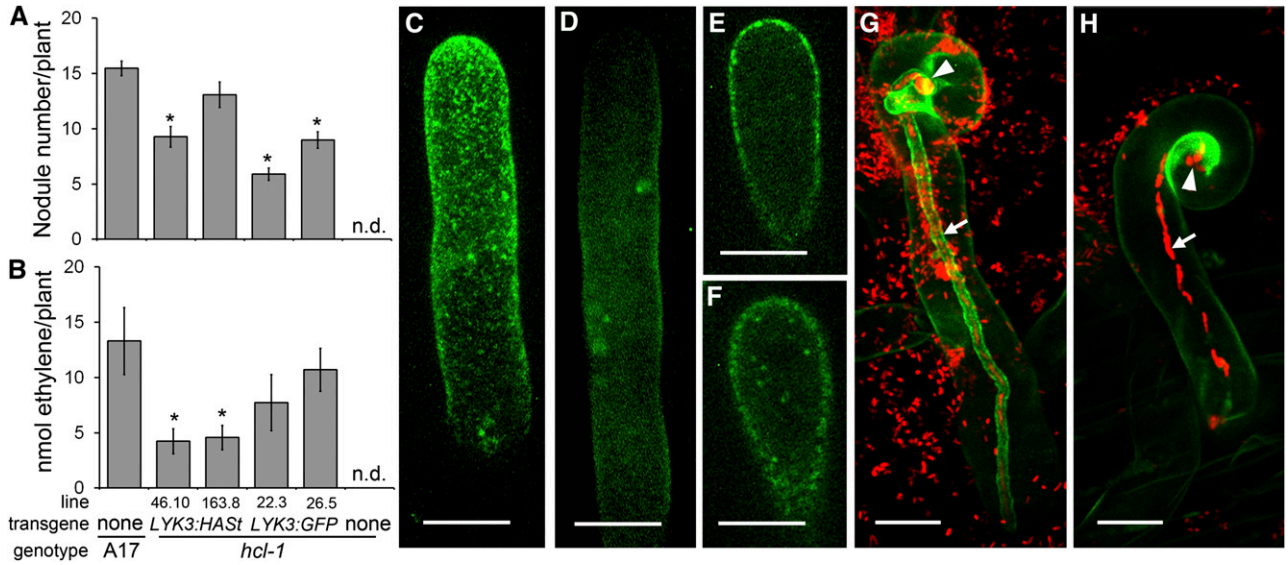

Figure 1. Tagged LYK3 Complements the *hcl-1* Mutant and Has a Punctate Distribution at the Cell Periphery and along Infection Threads.

(A) and **(B)** Approximately 30 plants per genotype were assayed for nodulation and acetylene reduction phenotypes at 21 d after inoculation; error bars represent SE. *P < 0.05 by two-tailed *t* tests; n.d., not detected.

(A) Average nodule number.

(B) Acetylene reduction assays show that nodules on transgenic lines are able to fix nitrogen at 21 d after inoculation (Turner and Gibson, 1980).

(C) to **(H)** *M. truncatula* stable transgenic lines transformed with *pLYK3:LYK3:GFP* (line 22.3; **[C]** and **[E]** to **[G]**) or *pLYK3:LYK3:HASt* (line 46.10; **[D]** and **[H]**). Bars = 10 μm.

(C) In uninoculated root hairs, LYK3:GFP localized to puncta in a gradient from the cell tip as shown by the brightest point projection of a confocal stack.

(D) Root hair autofluorescence in the LYK3:HASt line shown by a brightest-point projection of a confocal stack (same exposure settings as **[C]**).

(E) A single optical section revealed that the label is primarily at the extreme periphery of the cell. A few labeled vesicles were also observed in the cytoplasm that fills the tips of these cells (see Supplemental Figure 1 online).

(F) By 6 HAI, cytosolic organelles labeled with LYK3:GFP were visible.

(G) and **(H)** Arrowheads mark the infection thread initiation site in curled root hairs; arrows mark the infection thread. Bars = 10 μm.

(G) LYK3:GFP (green) was visible along infection threads 4 d after treatment with P_{trp}-*mCherry*–expressing *S. meliloti* (red) in a brightest-point projection of a confocal stack.

(H) No fluorescence was visible on infection threads of plants expressing *LYK3:HASt*.

clearly distinguishable from autofluorescence in the LYK3:HASt transgenic line 46.10 (Figure 1D). The signal was brighter in the LYK3:GFP line 22.3, so this is used for all subsequent imaging studies involving stable transgenic plants. A few labeled vesicles were visible in the cell interior (Figure 1E; see Supplemental Movie 1A online). In hairy roots, there was little colocalization of LYK3:GFP with a dsRed cytoplasmic marker (see Supplemental Figure 1 online). The LYK3:GFP signal followed the membrane after plasmolysis (see Supplemental Figure 2 online), confirming that the labeled protein was not localized to the cell wall. These observations suggest that the majority of LYK3:GFP signal is plasma membrane associated, either in the plasma membrane itself or in membrane-tethered vesicles that cannot be resolved from the membrane by light microscopy. A plasma membrane–associated localization is consistent with previous reports of LYK3 localization when the protein was overexpressed in *Nicotiana benthamiana* leaf cells (Lefebvre et al., 2010; Mbengue et al., 2010; Klaus-Heisen et al., 2011).

Native GFP forms weak dimers. To determine if dimerization of the GFP tag could account for the punctate appearance of LYK3, we generated a *pLYK3:gLYK3:mYFP* construct (monomeric yellow fluorescent protein [mYFP] contains an A206K mutation that abolishes dimerization; Zacharias et al., 2002) and introduced it into wild-type A17 roots using *A. rhizogenes*–mediated hairy root transformation. We found that mYFP-tagged LYK3 is also punctate and localizes to the extreme cell periphery (see Supplemental Figure 3 online). This result indicates that the punctate appearance of tagged LYK3 is not an artifact of tag dimerization.

LYK3:GFP Is Associated with Infection Threads

Following treatment of roots with an *S. meliloti* strain producing constitutive high levels of NF (Fisher et al., 1988), an increase in LYK3:GFP vesicles in the cell interior was evident by 6 h after inoculation (HAI) (Figure 1F; see Supplemental Movie 1B online) and persisted at 24 HAI. No consistent increase in vesicles was evident at 0.5 or 3 HAI (data not shown).

By 4 d after inoculation with *S. meliloti*, we observed LYK3:GFP along infection threads in root hairs in stable transgenic lines (Figure 1G) and hairy roots (see Supplemental Figure 4 online). By analogy to LYK3:GFP localization in plasmolyzed root hairs (see Supplemental Figure 2 online), we infer that LYK3:GFP is

not localized to the infection thread wall. No infection thread–associated fluorescent signal was visible in control plants expressing LYK3:HASt (Figure 1H), although pronounced autofluorescence was visible in the crooks of curled root hairs. We did not detect LYK3:GFP associated with infection threads in interior nodule cells (see Supplemental Figure 5 online). Consistent with this observation, we found that *LYK3* expression was weak to absent in the infection zone of nodules using a *pLYK3*:β-glucuronidase (*GUS*) reporter (see Supplemental Figure 6 online). This expression is similar to previous reports of *LYK3* promoter activity (Limpens et al., 2005; Mbengue et al., 2010).

LYK3:GFP Displays a NF-Dependent Change in Mobility after Bacterial Inoculation

We observed that in the absence of bacteria, the distribution of LYK3:GFP at the plane of the membrane is dynamic (Figure 2; see Supplemental Movie 2 online). Whereas lateral mobility of signal appears evident by inspection of time series data (see Supplemental Movie 2 online), the density of GFP-labeled LYK3 is too high and the rate of acquisition required to detect LYK3:GFP is too slow for reliable tracking of individual puncta. An alternative method to assess mobility is analysis of signal fluctuation over time. For example, the punctate appearance of LYK3:GFP is maintained in a three-frame average (6 s; Figure 2) but is lost in a 90-frame average (180 s). LYK3:GFP dynamics can also be observed by monitoring the signal intensity along a line over time and displaying it as a kymograph (Figure 2); an absence of vertical streaks in the kymograph indicates that the signal fluctuates rapidly at all locations, consistent with rapid mobility of the LYK3:GFP.

We observed the distribution of LYK3:GFP puncta in root hairs 24 HAI with wild-type *S. meliloti* strain Rm1021 (pretreated with 3 μM luteolin). In the majority of branched or curled root hairs (n = 17/24 root hairs), LYK3:GFP puncta became stable over minutes (Figure 2; see Supplemental Movie 2 online). Individual LYK3:GFP puncta are still apparent in a 90-frame average. Increased puncta stability is evident in the increased structure in the kymograph; vertical streaks represent puncta that are stable in position over the 3-min time series (Figure 2).

To determine if the shift in LYK3:GFP mobility is dependent on bacterial NF and NF structure, we treated plants with purified NF (Ehrhardt et al., 1992), with a bacterial mutant unable to make the *N*-acetyl glucosamine backbone of NF (*ΔnodD1ABC*; Fisher et al., 1988) and with mutant bacteria that produce NFs with altered structures (*nodH*:Tn*5* and *ΔnodF,nodL*:Tn*5*; Ardourel et al., 1994; Wais et al., 2002). All strains were grown in the presence of 3 μM luteolin to induce NF production. NF-deficient bacteria and purified NF were not sufficient to cause increased stability of LYK3:GFP puncta (Figure 2; see Supplemental Movie 2 online). NF was applied at 10 nM, a concentration that induces both tip-localized calcium flux and cellular calcium spiking (Shaw and Long, 2003) and significant root hair deformation (Figure 2). We found no change in LYK3:GFP mobility in response to the *nodH* mutant (Figure 2; see Supplemental Movie 2 online). By contrast, the *nodFL* double mutant caused a shift in LYK3:GFP mobility in the majority of root hairs (n = 15/22; Figure 2; see Supplemental Movie 2 online). These results indicate that a sulfated product of *nod* gene activity is necessary for the shift in LYK3:GFP mobility, but NF nonreducing end modifications are dispensable for this effect.

FLOT4 and LYK3 Have Increased Colocalization after Bacterial Inoculation

An *M. truncatula* flotillin protein, FLOT4, is a predicted peripheral membrane protein that has a punctate plasma membrane–associated distribution similar to LYK3 (Haney and Long, 2010). *FLOT4* and *LYK3* genes have similar RNA interference phenotypes and gene expression patterns (Smit et al., 2007; Haney and Long, 2010; Mbengue et al., 2010). This implies that the two may function cooperatively to mediate symbiotic infection. To test if tagged FLOT4 and LYK3 puncta are codistributed, we generated hairy roots expressing *pFLOT4*:*gFLOT4*:*mCherry* in the *hcl-1* mutant stably transformed with *pLYK3*:*gLYK3*:*GFP*.

In buffer-treated root hairs, FLOT4:mCherry and LYK3:GFP showed a limited overlap in distribution but had distinct dynamic behaviors (Figures 3 and 4, left panels). Using three-dimensional (3D) image volumes acquired at the root hair cell tip, we calculated Pearson's correlation coefficients (r) in voxels (Costes et al., 2004). In buffer-treated root hairs, $r = 0.15 \pm 0.03$, indicating that FLOT4 and LYK3 colocalize only slightly more often than is predicted by an uncorrelated distribution of the proteins (r = 0 for an uncorrelated distribution). Time-lapse imaging revealed that bright FLOT4 puncta were relatively stable whereas the majority of LYK3 puncta were dynamic (Figures 4A to 4C; see Supplemental Movie 3 online). FLOT4 and LYK3 signal intensities were observed along linear transects of the time-averaged images (Figures 4D and 4E). These results show that in buffer-treated roots, there is little correlation of average LYK3 and FLOT4 position and intensity.

Inoculation with *S. meliloti* had a pronounced effect on FLOT4 and LYK3 colocalization in root hair cells at 24 h (Figure 3, right panels). Both the positions and relative intensities of stable LYK3:GFP puncta were well correlated with FLOT4:mCherry puncta (Figure 4, compare left and right panels; see Supplemental Movie 4 online). In cells that reinitiated tip growth, FLOT4 and LYK3 colocalization rose sharply (Figure 3C; $r = 0.66 \pm 0.03$; $P = 5 \times 10^{-15}$). In inoculated root hairs that had not reinitiated tip growth (swollen or no visible response), we observed an increase in colocalization compared with buffer treated roots, although to a lesser degree ($r = 0.40 \pm 0.05$; $P = 1 \times 10^{-4}$). As observed with FLOT4:GFP (Haney and Long, 2010), FLOT4:mCherry became distributed in more spots by 24 HAI and redistributed to form a cap at the cell tip (Figure 3A). LYK3:GFP vesicles were evident in the cytoplasm of these root hairs, but these vesicles were not marked by FLOT4:mCherry (see Supplemental Figure 7 and Supplemental Movie 5 online).

The LYK3 Mutant *hcl-1* Displays a Nonsymbiotic Defect in Root Hair Elongation

During the course of our localization studies, we found that *hcl-1* mutant plants have a root hair elongation defect on Fåhraeus media (used for generation of hairy roots) that is reminiscent of root hair elongation defects in the ethylene insensitive mutant

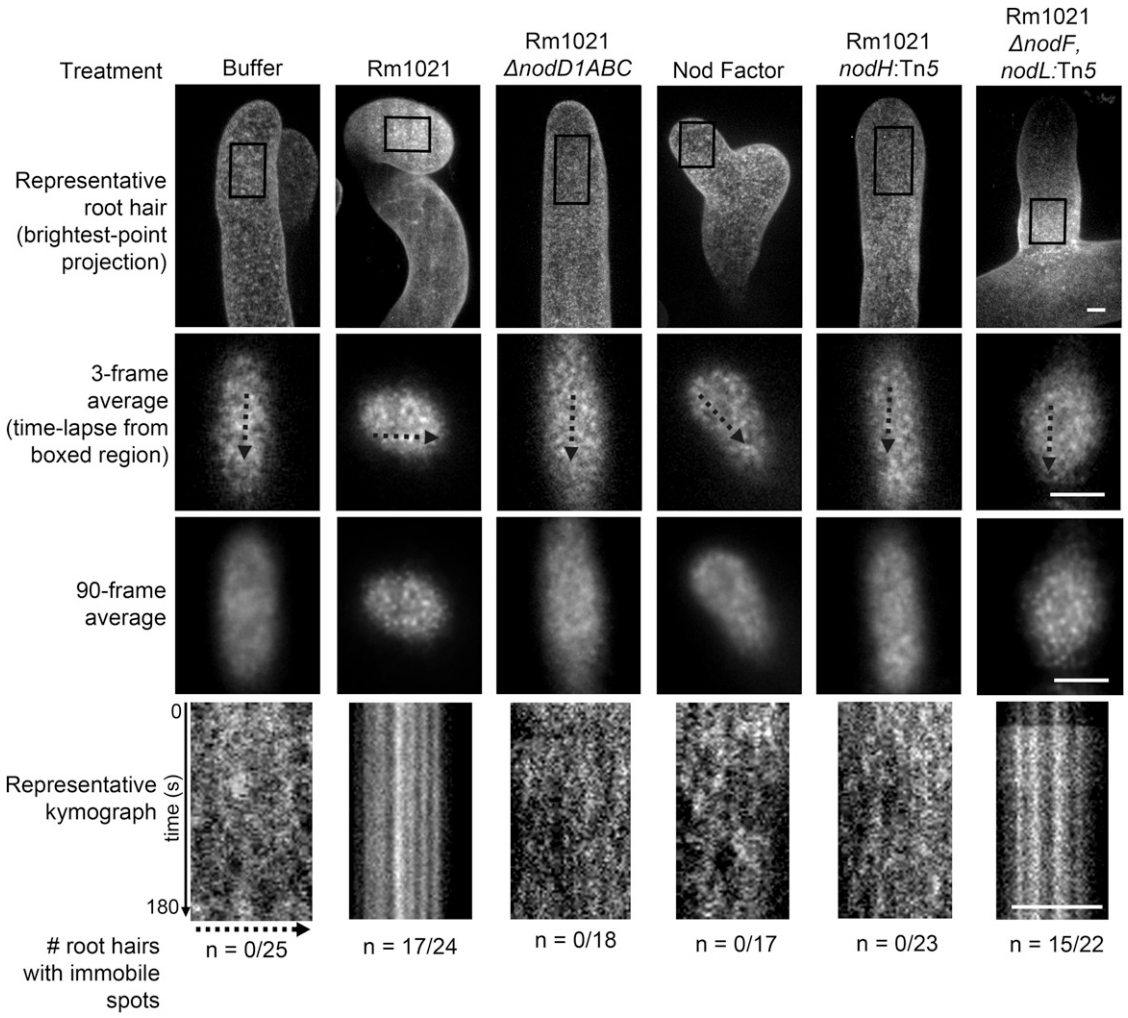

Figure 2. LYK3:GFP Puncta Show a NF-Dependent Shift in Mobility upon Bacterial Inoculation.

Localization and time-lapse images of LYK3:GFP mobility 24 HAI with buffer, wild-type *S. meliloti* Rm1021, Rm1021 unable to make the NF backbone (*ΔnodD1ABC*), purified Rm1021 NF, or strains that lack NF sulfation (*nodH*:Tn*5*) or lack acetylation and have an altered fatty acid chain (Rm1021 *ΔnodF*, *nodL*:Tn*5*). Time-lapse images, taken at 2-s increments, are single optical sections taken at the plane of the membrane from the boxed region in the top panel. Buffer-treated root hairs maintain the punctate appearance of LYK3:GFP (three-frame average) but are mobile as indicated by the loss of punctate appearance in a 90-frame average. Kymographs show the signal intensity over position (selection marked by arrows in three-frame average images). The unstructured appearance in the buffer-treated root hair kymograph shows that on average, LYK3:GFP puncta are not stable over time. Treatment with wild-type Rm1021 bacteria causes a mobility shift represented by the increase in punctate appearance in the 90-frame average and the structured pattern shown in the kymograph. Bacteria unable to make the NF backbone do not trigger the shift in LYK3:GFP mobility. NF alone was not sufficient to trigger the shift in LYK3:GFP mobility nor was a *nodH*:Tn*5* mutant. A *ΔnodF*,*nodL*:Tn*5* mutant caused a shift in LYK3:GFP mobility in some root hairs. A count of root hairs with immobile spots, per total number of root hairs observed, is indicated for each treatment. Root hairs were observed for at least five independent plants per treatment; images were taken at 2-s increments. Scale bars (3 μm) on far right panels apply to all images in the row.

ein2 (see Supplemental Figure 8 online; Pitts et al., 1998). The root hair phenotype was not observed on the buffered nodulation medium (BNM) media that is typically used for nodulation assays (data not shown) nor was it observed with *hcl-2*, *hcl-3*, or *hcl-4* mutant alleles of *LYK3* (see Supplemental Figure 8 online). Our transgenic lines were constructed in the *hcl-1* mutant background, and we found that *LYK3*:*GFP* and *LYK3*:*HASt* transgenes complemented the *hcl-1* root hair elongation defect (see Supplemental Figure 8 online).

FLOT4 Mislocalizes in a *LYK3* Mutant

In response to *S. meliloti* treatment, FLOT4:GFP redistributes to form a bright cap at the tip of responding root hairs (Haney and Long, 2010). To test whether this redistribution depends on *LYK3*, we generated hairy roots expressing *FLOT4*:*GFP* on plants containing mutations in *LYK3* or mutations in the symbiotic receptors *DMI2* and *NFP*. We first observed protein distribution in uninoculated plants. Compared with wild-type plants,

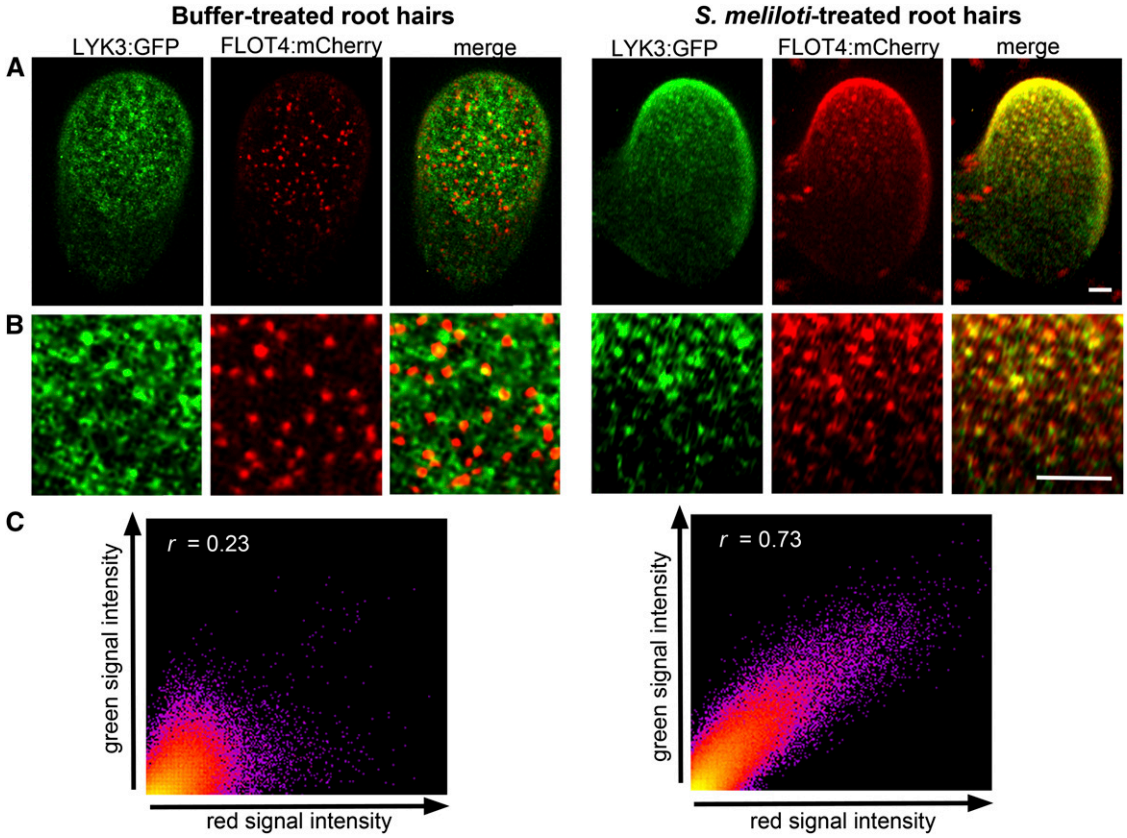

Figure 3. LYK3 and FLOT4 Colocalize in Inoculated Root Hairs in 3D Space.

(A) Codistributions of FLOT4:mCherry and LYK3:GFP signals in 3D space; z-stacks were obtained at 0.3-μm increments from the top 15 μm of root hairs.

(B) Higher magnification of images in **(A)**.

(C) Pearson's correlation coefficients (*r*) for 3D voxel intensities were calculated from two-dimensional correlation plots (Costes et al., 2004). Left panels: buffer-treated root hairs ($r = 0.15 \pm 0.03$; $n = 23$ root hairs [four plants]). Right panels: 24 HAI with bacteria, a significant increase in codistribution was observed ($r = 0.66 \pm 0.03$; $n = 22$ root hairs [four plants]; $P = 5 \times 10^{-15}$). Maximum intensity projections, correlation plots, and *r* values of representative root hairs are shown. Scale bars (2 μm) on far right panels apply to all images in the row.

the density of FLOT4:GFP puncta decreased in root hairs and epidermal cells of the *LYK3* mutant *hcl-1* (kinase-inactive allele). FLOT4:GFP puncta density was similar to the wild type in *nfp-1* (predicted null allele) and *dmi2-4* (predicted kinase-inactive) genetic backgrounds (Figures 5A to 5D and 5H; see Supplemental Figure 9 online). We found no significant difference between overall FLOT4:GFP signal intensity in the wild type compared with *hcl-1* plants, indicating that a decrease in protein abundance cannot account for the decrease in spot density (see Supplemental Figure 9K online). We also compared the pattern of FLOT4:GFP protein location in wild-type and mutant plants. In wild-type plants, FLOT4 puncta do not demonstrate marked polar distribution in epidermal cells and root hairs (Haney and Long, 2010). In *nfp-1*, *dmi2-4*, and *hcl-1* plants, we observed an increase in FLOT4:GFP signal at the apical pole of epidermal cells ($P < 0.01$; see Supplemental Figure 9 online).

To determine if the observed decrease in FLOT4:GFP puncta density is a consequence of altered root hair morphology in the *hcl-1* mutant, we expressed *FLOT2:GFP* in the *hcl-1* mutant background. *M. truncatula* FLOT2 also localizes to membrane-associated puncta and is required for symbiosis but not for infection thread elongation (Haney and Long, 2010). We found no decrease in FLOT2:GFP puncta density in root hairs or epidermal cells relative to FLOT2:GFP in wild-type plants (Figures 5F and 5G; see Supplemental Figure 9 online). FLOT2:GFP normally shows marked polar localization in epidermal cells; however, we observed no increase in polar localization when *FLOT2:GFP* was expressed in the *hcl-1* background (see Supplemental Figure 9 online). Thus, the decrease in spot density of FLOT4:GFP is not due to a general perturbation of protein distribution in the *hcl-1* mutant and increased polar localization is specific to FLOT4:GFP.

The *hcl-1* mutant allele harbors a single-base substitution within the highly conserved ATP binding pocket of the LYK3 kinase domain, which abolishes kinase activity (Klaus-Heisen et al., 2011). By contrast, the *hcl-2* and *hcl-4* alleles contain mutations in first intron splice sites and result in altered *LYK3* transcripts that encode mutated proteins; the weaker allele *hcl-4* contains ~8% wild-type *LYK3* transcripts (Smit et al., 2007). We

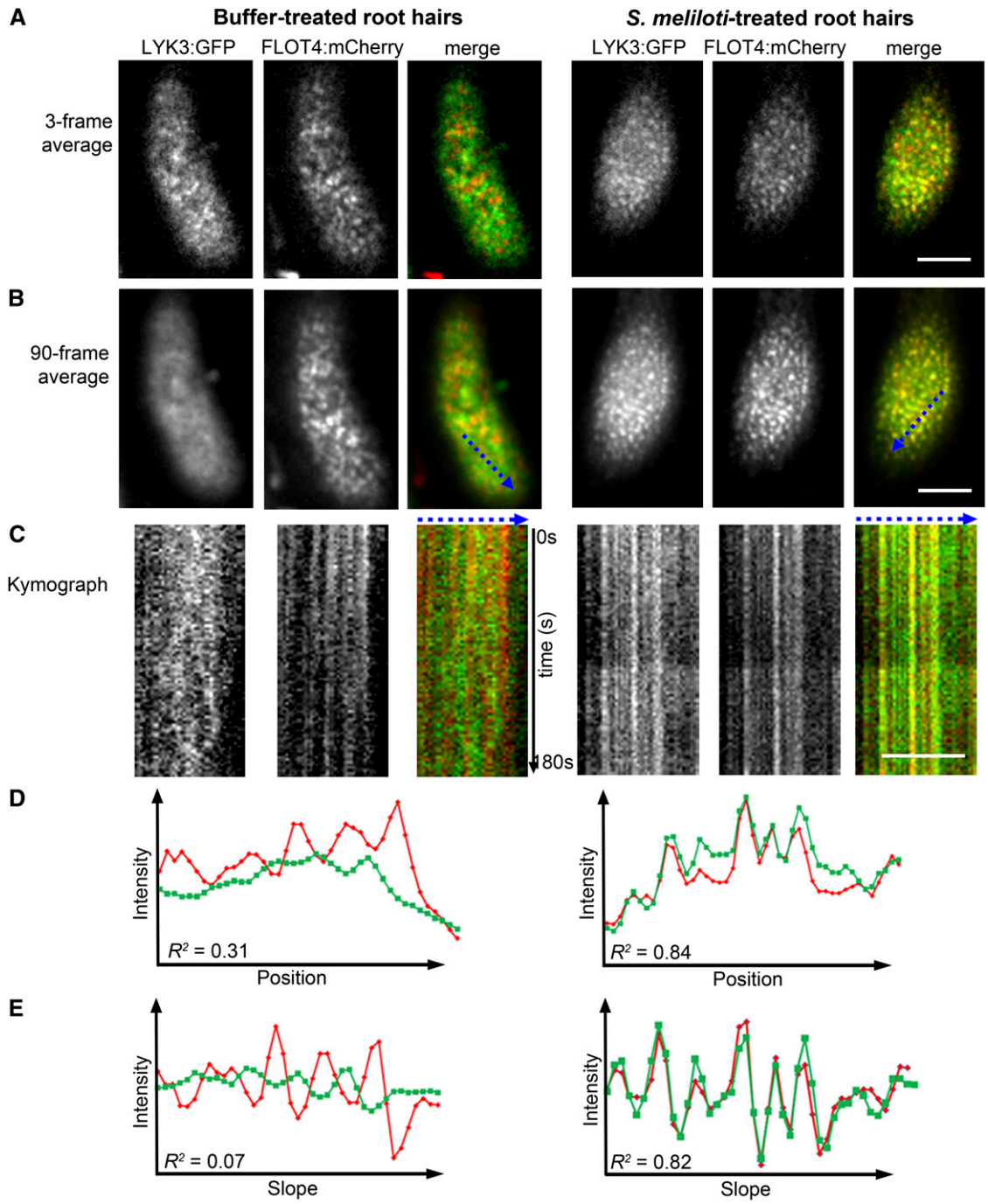

Figure 4. After Inoculation, LYK3 Puncta Shift from Dynamic to Stable.

Time-series images of FLOT4 and LYK3 after buffer or bacterial treatment acquired at 2-s intervals for 180 s.
(A) Three-frame averages show that the punctate distributions for LYK3 and FLOT4 are maintained in the absence or presence of bacteria.
(B) Ninety-frame averaged images are shown; diffuse signals are indicative of mobile puncta, whereas discrete spots designate stable puncta.
(C) Kymographs of intensities in 90-frame time-series images (dashed blue line in **[B]**). In the absence of bacteria, LYK3:GFP was dynamic and individual puncta were unstable, producing an unstructured pattern in the kymograph. FLOT4 puncta were relatively stable and yielded vertical streaks. In the presence of bacteria, both LYK3 and FLOT4 puncta were stable and created vertical streaks in the kymographs. In **(A)** to **(C)**, bars (3 μm) on far right panels apply to all images in the row.
(D) Signal intensities from FLOT4:mCherry (red) and LYK3:GFP (green) signals along linear transects of the time-averaged images (dashed blue lines) are shown graphically. In the absence of bacteria, there is little correlation of average LYK3 and FLOT4 position and intensity ($R^2 = 0.27 \pm 0.06$; $n = 12$

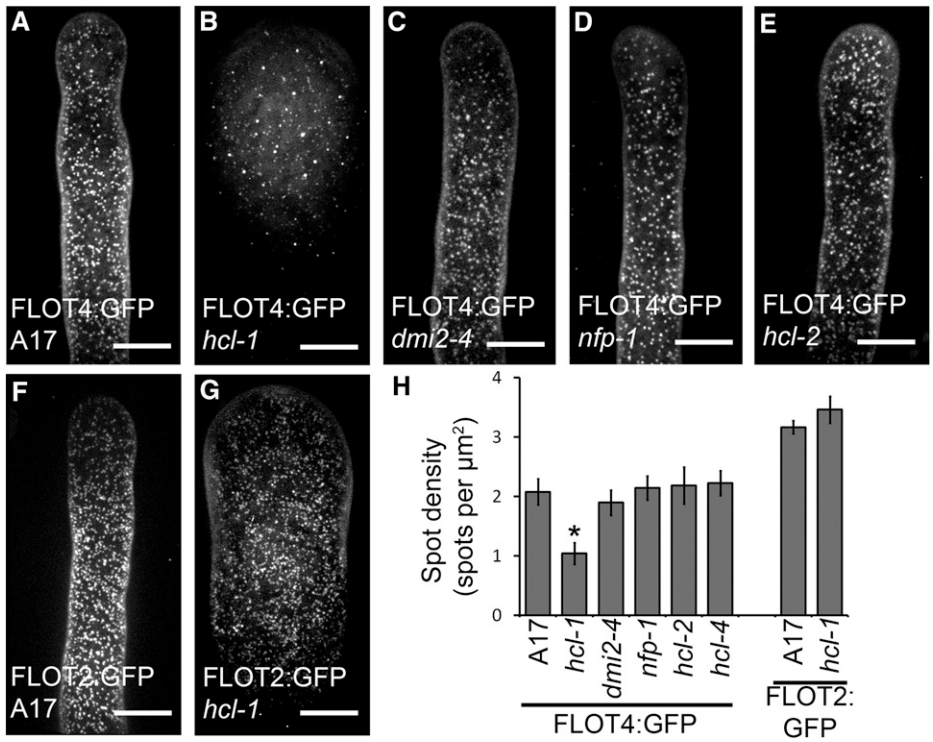

Figure 5. FLOT4:GFP Mislocalizes in a Kinase-Inactive Mutant of LYK3, *hcl-1*.

(A) to **(E)** Hairy roots transformed with *pFLOT4:gFLOT4:GFP*. FLOT4:GFP puncta in wild-type (A17) **(A)**, *hcl-1* **(B)**, *dmi2-4* **(C)**, *nfp-1* **(D)**, or *hcl-2* **(E)** root hair cells. Bars = 10 μm.

(F) and **(G)** Hairy roots transformed with *35S:gFLOT2:GFP*. FLOT2:GFP puncta in wild-type (A17) **(F)** or *hcl-1* **(G)** root hairs. Images are maximum intensity z-projections of ~45 optical sections taken at 0.3-μm increments. Bars = 10 μm.

(H) Decreased spot density was specific to FLOT4:GFP in the *hcl-1* mutant background. Maximum intensity z-projections were used for analyses; $n \geq 15$ cells (from at least three plants). Error bars represent ± SE; *P < 0.001.

tested if decreased FLOT4:GFP puncta density was specific to the *hcl-1* allele or if it also occurred in the *LYK3* splice mutants. The density of FLOT4:GFP puncta in *hcl-2* and *hcl-4* was indistinguishable from that in wild-type root hairs and epidermal cells (Figures 5E and 5H; see Supplemental Figure 9 online). We also assessed FLOT4 distribution and found FLOT4:GFP had a more polar distribution in *hcl-2*, whereas localization in *hcl-4* was indistinguishable from wild-type roots (see Supplemental Figure 9 online).

Because the *hcl-1* mutant was used as the background for LYK3:GFP localization and LYK3:GFP/ FLOT4:mCherry codistribution, we investigated whether LYK3 transgenes rescued FLOT4:GFP distribution in *hcl-1* roots. We found that like FLOT4:GFP, FLOT4:mCherry displayed both a decrease in density of FLOT4:mCherry puncta and a polarity defect in epidermal cells in the *hcl-1* mutant background. The *pLYK3:gLYK3:GFP* transgene complemented only the density phenotype (see Supplemental Figure 10 online). The function of flotillin polarity is unknown; since the LYK3:GFP transgenic lines form functional nodules, this suggests polar distribution may not be relevant for the symbiotic activity of FLOT4. Additionally, codistribution was assessed in root hairs, where FLOT4:GFP distribution appears to be normal.

DISCUSSION

A Previously Uncharacterized Cellular Behavior Is a Marker for Early Symbiotic Events

Root hair curling, membrane depolarization, calcium spiking, and transcriptional changes provide markers for dissecting early

Figure 4. (continued).

transects [three plants]). With bacterial treatment, both the position and the relative intensity of the puncta are correlated (R^2 = 0.85 ± 0.02; n = 16 transects [four plants]; P = 1 × 10^{-10}).

(E) Slope versus intensity plots for charts in **(D)** are shown. These show that the rate of change in signal intensity as a function of position is well correlated between FLOT4:mCherry and LYK3:GFP only in the presence of bacteria. In buffer-treated root hairs, R^2 (*slope*) = 0.10 ± 0.03; in bacteria-treated root hairs, R^2 (*slope*) =0.74 ± 0.02; P = 4 × 10^{-13} by two-tailed *t* test.

events during rhizobia-legume symbiosis. Within the first day of bacterial inoculation, we observed that LYK3:GFP puncta undergo a *nod* gene–dependent change in mobility, indicating that this is among the early cellular responses to perception of symbiotic bacteria. We found that exogenously supplied NF is not sufficient for the shift in LYK3 mobility. This suggests that either (1) a localized delivery of NF by a live bacterium is required for the change in LYK3:GFP puncta dynamics or (2) that in addition to NF, a second signal is required. As exogenously supplied NF is not sufficient to induce infection thread formation, both possibilities have interesting implications for the infection process.

Like calcium spiking, the change in LYK3:GFP puncta dynamics appears to be dependent on NF sulfation but not on the species-specific modifications to the nonreducing end of the molecule (Wais et al., 2002). Genetic studies predict that LYK3 regulation of infection requires *nodFL*-dependent NF modifications (Smit et al., 2007). Because the *nodFL* mutant is able to induce a shift in LYK3:GFP dynamics, the requirement for *nodFL* in infection is not due to a defect in LYK3 immobilization. The NFP receptor is insensitive to nonreducing end modifications of NF but sensitive to NF sulfation (Wais et al., 2000, 2002). Our observations are consistent with a role of the NFP/DMI signaling pathway in LYK3 immobilization.

Our data show that after bacterial treatment, LYK3 immobilization occurs at many sites throughout responding root hair cells (Figures 2 and 4; see Supplemental Movies 2 and 4 online). In general, infection thread initiation only occurs at one site per cell; not all sites of immobile LYK3 will form infection threads. The role of LYK3 immobilization in infection is consistent with a two-step process in which LYK3 is first immobilized and then a single LYK3 spot per cell is activated to initiate infection. This model predicts that infection threads will initiate at the site of a single immobile LYK3 spot.

Our observations are also consistent with LYK3 immobilization acting to negatively regulate LYK3 function. Sequestering an inactive form of LYK3 away from the infection site could serve to block LYK3 from interacting with other proteins involved in infection or prevent multiple infection events per cell. It is also possible that the responding root hairs where LYK3 remained mobile (Figure 2; LYK3 was found to be immobilized in 17 out of 24 root hairs) are root hairs that eventually support bacterial infection. This model predicts that infection threads will initiate either at a location without immobile LYK3 puncta or in a cell where LYK3 remains mobile.

LYK3 Is Present on Intracellular Vesicles and Infection Threads after Inoculation

We observed an increase in the pool of intracellular vesicles that contain LYK3:GFP by 6 h after treatment with *S. meliloti*. The origin of these vesicles is unknown; they may arise from endocytosis of LYK3:GFP from the membrane, release of LYK3:GFP vesicles that may have been tethered to the plasma membrane, or from new protein synthesis and packaging into secretory compartments. The behavior of LYK3 is distinct from the ligand-dependent endocytosis observed with the plant flagellin receptor FLS2 (Robatzek et al., 2006). FLS2 internalization followed by rapid degradation occurs within minutes of ligand application. By contrast, we observed persistence of LYK3:GFP for days after bacterial application. If LYK3 is internalized from the membrane and degraded, this must be accompanied by new protein synthesis to maintain the levels of LYK3 that we observed during infection. FLS2 internalization is likely dependent on ubiquitination (Salomon and Robatzek, 2006). Interestingly, LYK3 interacts with PUB1 E3 ubiquitin ligase, which negatively regulates nodulation by an unknown mechanism (Mbengue et al., 2010).

LYK3 is required for initiation and continued growth of infection threads (Limpens et al., 2003; Smit et al., 2007). We found that LYK3:GFP is present in elongating root hairs prior to interaction with bacteria and persists in association with infection threads in root hairs. LYK3 localization supports the genetic requirement for LYK3 in NF perception and early infection. We did not detect LYK3:GFP associated with infection threads in interior nodule cells (see Supplemental Figure 5 online). This is consistent with *LYK3* promoter activity and expression data that shows *LYK3* expression is weak to absent in the infection zone of nodules (Limpens et al., 2005; Mbengue et al., 2010; see Supplemental Figure 5 online). Several models are consistent with the apparent absence of the LYK3 protein on infection threads in subepidermal and inner nodule layers: (1) LYK3 is present at low levels that are sufficient for NF perception in nodules or (2) NF perception by LYK3 is not required for later stages of infection.

We also observed a conditional defect in root hair elongation in the kinase-inactive allele of LYK3, *hcl-1*, that is dependent on the composition of growth medium; the phenotype can be complemented by a tagged wild-type version of LYK3, so the phenotype cannot be attributed to a background mutation in this plant line. This is the first nonsymbiotic phenotype reported for the *hcl-1* mutant (Figure 5; see Supplemental Figure 9 online). A distinct nonsymbiotic defect in the root hair touch response has been observed for *dmi2* mutants (Esseling et al., 2004). Unlike the *dmi2* root hair phenotype, the *hcl-1* mutant phenotype was specific to a kinase-inactive allele, indicating a recessive gain-of-function phenotype. Determining the media component responsible for triggering this phenotype in the *hcl-1* mutant may provide clues about LYK3 function.

A Genetic Interaction between FLOT4 and LYK3

We found that FLOT4:GFP puncta density is altered in epidermal and root hair cells of the LYK3 kinase-inactive mutant *hcl-1* (but unaltered in the predicted kinase-inactive mutant *dmi2-4* or other alleles of *hcl*). These results indicate that only when the kinase domain of LYK3 is present but nonfunctional does FLOT4 (but not FLOT2) show a decrease in puncta density. The per-cell FLOT4:GFP signal intensity is unaltered in the *hcl-1* mutant, indicating that more protein is present per spot. Taken alone, these results suggest that FLOT4 may be interacting with the kinase domain of LYK3. However, we found that FLOT4 and LYK3 have limited codistribution in the absence of bacteria. This observation might indicate that the hcl-1 protein has altered localization itself. Alternatively, FLOT4 and LYK3 may not directly interact, or limited interaction of LYK3 and FLOT4 may be sufficient to cause a change in FLOT4 distribution.

We also found that mutations in symbiotic receptors *nfp*, *dmi2*, and *lyk3* (*hcl*) result in increased polarity of FLOT4, whereas the

polarity of FLOT2 is unaffected in a *lyk3* mutant. This indicates that one or more symbiotic receptor(s) is required to keep FLOT4 evenly distributed or to prevent it from moving to a more polar distribution. LYK3:GFP rescued the symbiotic defect in the *hcl-1* mutant but not FLOT4 polar localization; this suggests that the polar localization may not be relevant for the symbiotic activity of FLOT4. Because relatively little is known about how polarity is established and maintained in plants, this effect may shed light on a feature of basic plant cell biology.

The most parsimonious explanation for increased proximity and similarity of dynamics of FLOT4 and LYK3 after bacterial treatment is that LYK3 and FLOT4 are components of a shared complex. An alternative is that FLOT4 and LYK3 colocalization arises because they occupy the same compartment (but do not necessarily interact), whether it be a plasma membrane–tethered vesicle or a microdomain in the plasma membrane.

Signal-Dependent Protein Redistribution

We found that after bacterial treatment, both FLOT4 and LYK3 redistribute and LYK3 has a change in dynamics. These data demonstrate that changes in protein architecture accompany altered root hair morphology during early symbiotic events. However, whereas LYK3 and FLOT4 are integral and peripheral membrane proteins, respectively, the specific membrane to which they localize has not been determined. Because LYK3 is peripheral to the bulk of the cell cytoplasm (see Supplemental Figure 1 online), it most likely localizes to the plasma membrane or to a plasma membrane–associated compartment. Membrane-associated compartments may include cytosolic vesicles that are tethered to the membrane or to cortical cytoskeletal elements (Gutierrez et al., 2009). Redistribution of LYK3 and FLOT4 after bacterial treatment may indicate a lateral move within the membrane, a change in localization of tethered vesicles, fusion of tethered vesicles with the plasma membrane, or internalization of proteins from the plasma membrane. The stability of the tagged LYK3 and FLOT4 signal after bacterial inoculation suggests that these proteins are not freely diffusing within the plasma membrane but rather are stabilized by a structure, such as the cell wall or cytoskeletal elements. The resolution of confocal microscopy is insufficient to distinguish between these possibilities; electron microscopy or other high-resolution methods are necessary to determine the exact localization of LYK3 puncta before and after inoculation with symbiotic rhizobia. Identification of the compartment(s) marked by FLOT4 and LYK3 prior to and during rhizobial symbiosis will provide insights into how the plant cell is reprogrammed for symbiosis.

METHODS

Plant Growth and Bacterial Treatments

Medicago truncatula Gaertner cv Jemalong A17, mutant lines *hcl-1*, *hcl-2* (Catoira et al., 2001), *hcl-4* (Smit et al., 2007), *dmi2-4* (Endre et al., 2002), *nfp-1* (Amor et al., 2003), and *skl1-2* (Penmetsa et al., 2008), and transgenic lines (this study) were grown, inoculated, and harvested as described (Mitra and Long, 2004).

Sinorhizobium meliloti strain Rm1021 is a streptomycin-resistant derivative of wild-type field isolate SU47 (Meade et al., 1982). For bacterial treatments, Rm1021, SL44 (Rm1021 Δ*nodD1ABC*; Fisher et al., 1988), RJW14 (Rm1021 Δ*nodF*, *nodL*:Tn*5*; Wais et al., 2002), JT210 (Rm1021 *NodH*:Tn*5*; Swanson et al., 1987), or Rm1021 overexpressing *nodD3* from the plasmid pRmE65 (Fisher et al., 1988) were grown overnight in Luria-Bertani medium (Meade et al., 1982) supplemented with antibiotics. Three to six hours prior to inoculation, luteolin was added to the bacterial cultures to a final concentration of 3 μM. Bacteria were grown to an OD_{600} between 0.5 and 1, then pelleted and resuspended in half-strength BNM (Ehrhardt et al., 1992). Rm1021 Nod Factor, NodRmIV (Ac, C16:2, 5), was purified as described (Ehrhardt et al., 1996). Transgenic plants were inoculated with 1 μL of bacteria (OD_{600} = 0.1) or 1 μL 10 nM NF 6 to 8 d after germination.

Construct Design

pLP100:*pLYK3*:*GUS* was created as follows: Primers BR323/324 used to amplify 2 kb upstream of the LYK3 coding sequence and TA cloned into pCR2.1 (Invitrogen). A *Bam*HI-*Nco*I fragment containing the *LYK3* promoter was excised from this construct and ligated into the corresponding sites of the binary vector pLP100 (Szabados et al., 1995) to generate a *pLYK3-GUS* fusion.

pLYK3:*gLYK3*:*GFP*:*mYFP* and :*HASt* were constructed as follows: The *LYK3* gene encompassing ~2 kb upstream of the start site through the last codon of the *LYK3* coding sequence was amplified from BAC MtH1-003I09 using primers BR412/413. These primers introduce unique *Xma*I and *Xho*I restriction sites immediately after the last codon. The resulting PCR product was directionally cloned into pENTR-D TOPO (Invitrogen). The stop codon and 500 bp of the LYK3 3′ untranslated region was amplified from the same BAC using primers BR398/399. These primers introduce an *Xma*I site immediately 5′ to the stop codon and an *Xho*I site on the 3′ end. This fragment was subsequently cloned into the *Xma*I and *Xho*I sites of the pENTR construct described above to generate *pENTR*:*pLYK3*:*gLYK3*. GFP, mYFP, and HASt tags were amplified using primer pairs BR391/392, CH435/436, or BR393/394, respectively, and the resulting PCR product was cloned into the unique *Xma*I site preceding the stop codon in *pENTR*:*pLYK3*:*gLYK3*. The GFP coding sequence originated from psmRSGFP (Davis and Vierstra, 1998), mYFP contains an A206K mutation to eliminate dimerization (Zacharias et al., 2002), and the HASt tag was generated in house and contains three tandem copies of the HA epitope translationally fused to the StrepII affinity tag (IBA). All constructs were confirmed by sequencing. The pENTR clones were recombined using LR Clonase (Invitrogen) with either pKGW-RR (Smit et al., 2005) for hairy root transformation or with *pMDC123*:*35S*:*GUSi* for stable transformation. *pMDC123*:*35S*:*GUSi* was created by ligating a *35S*:*GUSi*:*ocs* cassette into a unique *Hin*dIII site in the pMDC123 T-DNA (Curtis and Grossniklaus, 2003). Primers were as follows: BR323, 5′-GATCCATGGAATCAAGAAGAGAGAGAGAAAGAG-3′; BR324, 5′-TGTGTCTAAAATTAACAAAGATATTTTATGG-3′; BR391, 5′-AACCCGGG-*GGAGGT***ATG**AGTAAAGGAGAAG-3′; BR392, 5′-AACCCGGGTTATTT-GTATAGTTCATCCATGCCATG-3′; CH435, 5′-AAACCCGGG**ATG**GT-GAGCAAGGGCGAGGAG-3′; CH436, 5′-AAACCCGGGTTACTTGT-ACAGCTCGTCCATG-3′;BR393, 5′-ACCCGGGTACCCATACGATGTT-CCAG-3′; BR394, 5′-ACCCGGGTCACTTTTCGAATTGTGGATG-3′; BR398, 5′-CACCCGGGTGAAGATTTTGTGTGACAAATTG-3′; BR399, 5′-ACCTCGAGGTGAATTCCATTGTTTGG-3′; BR412, 5′-CACCTGTG-TCTAAAATTAACAAAGATATTTTATGG-3′; and BR413, 5′-CACTCGAG-ACCCGGGTCTAGTTGACAACAGATTTATGAGAG-3′.

Plasmids pCH153 containing *pFLOT4*:*gFLOT4*:*mCherry* and pCH046 containing *35S*:*FLOT2*:*mCherry* were generated by replacing GFP in plasmids pCH118 and pCH035 (Haney and Long, 2010) with mCherry: *mCherry* was amplified with primers 5′-AAACCCGGGATGGTGAG-CAAGGGCGAGGAG-3′ and 5′-AAATCTAGATTACTTGTACAGCTCGT-CCATG-3′ and inserted into the *Xma*I and *Xba*I sites in pCH118 and pCH035 (Haney and Long, 2010).

pQDN01 containing P_{trp}-*cyan fluorescent protein* (*CFP*) was constructed by replacing GFP in pDG71 (Gage, 2002) with CFP. pQDN03 was constructed by replacing *GFP* in pDG71 with *mCherry* (Haney and Long, 2010). Both *mCherry* and *CFP* were amplified using the forward primer 5′-TTTGGATCCACC**ATG**GTGAGCAAGGGC-3′ and reverse primer 5′-TTTTCTAGATTACTTGTACAGCTCGTCCATGC-3′. PCR products were digested with *Bam*HI and *Xba*I and ligated into the corresponding sites in pDG71.

Generation of Transgenic Plants

Seeds of *M. truncatula* cv Jemalong mutant *hcl-1* (Catoira et al., 2001) were scarified in concentrated sulfuric acid for 10 min, rinsed in sterile distilled water, and surface sterilized for 15 min in 1.2% (v/v) sodium hypochlorite solution containing 5 μL Tween 20. Seeds were rinsed in sterile water and then redried in a laminar flow hood and stored at 2 to 8°C until needed. Seeds were plated onto Schenk and Hildebrandt basal salt medium (SH) (Schenk and Hildebrandt, 1972) (Phytotechnology Labs) supplemented with Murashige and Skoog (MS) vitamins, 10 g/L Suc, 1.0 mg/L benzylaminopurine (BAP), 1.3 g/L calcium gluconate, and 8 g/L phytoagar (PlantMedia), pH 5.8, at a density of 40 seeds per plate. Seeds were cultured for 5 d at 30°C under a 16-h photoperiod (30 μmol/m^2s^2 T5 cool white lights).

Agrobacterium tumefaciens strain EHA105 carrying the appropriate binary vector was grown overnight at 28°C in MGL medium (5 g/L tryptone, 2.5 g/L yeast extract, 5 g/L NaCl, 5 g/L mannitol, 1.16 g/L glutamic acid, 0.25 g/L $K_2HPO_4{\cdot}3H_2O$, 0.1 g/L $MgSO_4$, and 1 g/L biotin, pH 7.0) supplemented with appropriate antibiotics . The *A. tumefaciens* culture was diluted 1:3 in TY medium, pH 5.5, supplemented with appropriate antibiotics and 200 μM acetosyringone and grown overnight. The overnight culture was diluted in TY medium to an OD_{600} of 0.4 to 0.5. Five-day-old germinating seedlings were transferred to a sterile 100 × 15-mm Petri dish containing 10 mL of the *A. tumefaciens* dilution. The seedling radicals were removed, leaving 3 to 5 mm of the hypocotyls, the cotyledons, and the shoot tip. The seedlings were bisected along the embryo axis generating two halves. After 10 min, the tissue was collected and plated with the cut edge in contact with the cocultivation medium consisting of SH medium supplemented with MS vitamins, 20 g/L Suc, 0.1 mg/L 1-naphthaleneacetic acid (NAA), 3.4 mg/L BAP, 1.3 g/L calcium gluconate, 8 g/L phytoagar, and 200 μM acetosyringone, pH 5.7 to 5.8. Tissue was incubated at 23°C in the dark for 5 d.

After 5 d, explants were collected and transferred to a temporary immersion bioreactor system (RITA; Sigma-Aldrich) containing 250 mL of SH medium supplemented with MS vitamins, 20 g/L Suc, 3.4 mg/L BAP, 0.1 mg/L NAA, 400 mg/L carbenicillin, 250 mg/L cefotaxime, 150 mg/L timentin, and 2 mg/L glufosinate. Explants were bathed in liquid induction medium at 4-h increments, six times per day, 2 min per submersion. Medium in RITA was replaced every 2 weeks with fresh medium of the same formulation. After three 2-week passages, explants were removed from the RITA and plated onto agar-solidified SH medium supplemented with MS vitamins, 20 g/L Suc, 3.4 mg/L BAP, 0.1 mg/L NAA, 400 mg/L carbenicillin, 250 mg/L cefotaxime, 150 mg/L timentin,1.3 g/L calcium gluconate, 8 g/L phytoagar, and 4 mg/L glufosinate. Tissue was subcultured to fresh medium of the same formulation every 14 d until small transgenic shoots developed. Once shoots were 5 mm in height, they were harvested and transferred to elongation medium consisting of SH medium supplemented with MS vitamins, 20 g/L Suc, 0.1 mg/L NAA, 1.3 g/L calcium gluconate, 8 g/L phytoagar 400 mg/L carbenicillin, 250 mg/L cefotaxime, 150 mg/L timentin, and 4 mg/L glufosinate.

To initiate rooting, elongated shoots were harvested and transferred to SH medium supplemented with MS vitamins, 20 g/L Suc, 10.0 mg/L NAA, 1.3 g/L calcium gluconate, 8 g/L phytoagar, 400 mg/L carbenicillin, 250 mg/L cefotaxime, and 4 mg/L glufosinate. After 3 d, shoots were removed from culture and transferred to a TKN1020 tray with 36-well plug flat inserts (ITLM) containing Sunshine Mix #1 (Sungro) and covered with 7.6 cm high humidity domes (ITLM). Plants were grown under a 16-h photoperiod at 26°C and 100 μmol/m^2 s^2 light. After 10 d, the 7.6-cm dome was replaced with a 15.3-cm dome. After an additional 10 d, the dome was removed. Seven days later, plants were transferred to the greenhouse.

Acetylene Reductions

Acetylene reduction (Turner and Gibson, 1980) was performed as described (Oke and Long, 1999). Plants were initially grown and inoculated on BNM plates as described above; at 21 d after inoculation, nodules were counted and the entire plant was moved to test tubes for the assays. At least four uninoculated plants were assayed per transgenic line to ensure that they did not have intrinsically higher levels of ethylene production.

Hairy Root Transformation

Plasmids were transformed into *Agrobacterium rhizogenes* Arqua1 (Quandt et al., 1993) and selected using the appropriate antibiotic. *A. rhizogenes*–mediated hairy root transformations were done according to Boisson-Dernier et al. (2001) with modifications described by Haney and Long (2010). After regeneration of hairy roots, plants were transferred to BNM with 0.1 μM aminoethoxyvinylglycine (AVG). Plants were flood inoculated 1 week later with 10 mL of the appropriate *S. meliloti* strain diluted to OD_{600} = 0.05 in half-strength BNM.

Histochemical GUS Assays

Plants were grown, harvested, and stained as described previously (Riely et al., 2007). pLYK3:GUS roots were imaged on a Leica DM5000B compound fluorescent microscope (JH Technologies) with a ×20 objective lens and differential interference contrast optics for GUS and a Y3 filter cube (excitation filter, BP 545/30; emission filter, BP 610/75) for the detection of mCherry. Images were collected using SPOT Advanced software version 4.1.

Confocal Microscopy

For infection thread localization studies, plants were inoculated with Rm1021 constitutively expressing *mCherry* or *CFP* from the plasmids pQDN03 or pQDN01. As the signal was brighter in the 22.3 LYK3:GFP than in the 26.1 line, possibly due to positional effects of the transgene, the 22.3 line was used for localization studies.

Root segments and nodule hand sections (for imaging the infection zone) were excised and mounted in BNM buffer, pH 6.5. Spinning disk confocal microscopy was performed on a system described previously (Gutierrez et al., 2009) using a ×100/1.4 numerical aperture oil immersion objective for root hair membrane imaging or a ×63/1.3 numerical aperture glycerol immersion objective for infection thread and nodule imaging. CFP, GFP, YFP, and dsRed/mCherry were excited at 442, 491, 515, and 561 nm, respectively, by solid-state lasers; emission filtering was accomplished with band-pass filters (470/40 for CFP, 530/50 nm for GFP, 570/65 for YFP, and 640/50 nm for mCherry/dsRed; Chroma Technology). Z-projections of root hairs are from ~100 images taken at increments of 0.3 μm (MCL NanoDrive). Time-lapse images were taken at 2-s increments. Stacks were processed using ImageJ software (http://rsbweb.nih.gov/ij/). Typical exposure times were 1000 ms for GFP and YFP, 300 ms for dsRed, 500 ms for mCherry, and 500 ms for CFP.

Brightest point z-projections of stacks of epidermal cells or root hairs were used for quantification of signal or density of spots. Final images included ~45 z-sections taken at 0.3-μm increments to cover just the top half (~15 μm) of epidermal cells. As a proxy for polarity, the ratio of signal density on the apical cell pole to the abaxial cell surface was determined as follows: (1) the average apical signal was measured by drawing a

1-pixel-wide line along the apical membrane and using ImageJ's Measure function to determine the average intensity per pixel (or signal density); (2) the abaxial signal was measured by a similar method but with a rectangular selection; and (3) the apical signal density was divided by the abaxial signal density to determine ratio of signal density. To measure density of flotillin puncta, images were automatically thresholded based on statistical distribution of signal so that just the puncta on the abaxial surface were defined. Using the "analyze particles" feature in ImageJ, the total number of spots was determined and divided by the total area measured to give a spot density. No constraints were placed on spot size or dimensions. At least five cells were measured from at least three independent plants for a total of at least 15 measurements per treatment. Significance was determined by two-tailed *t* test with equal variance.

Colocalization experiments were analyzed in 3D space using Imaris's (Bitplane) colocalization tool as described (Costes et al., 2004). Images were cropped in 3D to include ~20 μm of the growing root hair tip. The background thresholds were set at 1300 and 1080 for the green and red channels, respectively, and determined based on autofluorescence and background signals measured in LYK3:HASt plants cotransformed with an empty vector (pCH007; Haney and Long, 2010). The Pearson's correlation coefficient (*r*) was determined for correlation of voxel intensities in 3D space. Twenty-three buffer-treated root hairs were analyzed from four individual plants. Forty-three root hairs were analyzed on three independent inoculated plants, 21 of which had not reinitiated directional growth and 22 of which had. Two-tailed *t* tests with equal variance were used to determine significance of the differences in *r*.

Time-series data was acquired at 2-s intervals over a 3-min period. Analysis was done in ImageJ. Linear manual selections (1 pixel width) were made on average intensity projections and stacks to generate average pixel intensity and kymographs. Average pixel intensities were exported to Microsoft Excel to generate graphical representations and coefficients of determination (R^2). Slope at position x was approximated by the three-point estimation: $(f(x-h) - f(x+h))/2h$, where the step h was a single pixel. Two time-series data sets were analyzed from each of two independent inoculated or uninoculated roots (four images per treatment). Three selections were analyzed per root hair. Two-tailed *t* tests with equal variance were used to determine significance of the differences in R^2 values.

Accession Numbers

Sequence data from this article can be found in the GenBank/EMBL databases under the following accession numbers: LYK3 (AY372402), FLOT4 (GU224281), and FLOT2 (GU224279).

Supplemental Data

The following materials are available in the online version of this article.

Supplemental Figure 1. Tagged LYK3 Has Little Overlap with a Cytoplasmic Marker.

Supplemental Figure 2. The LYK3:GFP Signal Follows the Membrane after Plasmolysis.

Supplemental Figure 3. LYK3 Tagged with Monomeric YFP Appears Punctate.

Supplemental Figure 4. Tagged LYK3 Complements the *hcl-2* Infection Defect in Hairy Roots.

Supplemental Figure 5. LYK3:GFP Is Not Visible in the Infection Zone of Nodules.

Supplemental Figure 6. Localization of LYK3 Expression in Root Hairs and Nodules Using a LYK3 Promoter-GUS Fusion.

Supplemental Figure 7. FLOT4:mCherry Does Not Label LYK3:GFP Intracellular Vesicles.

Supplemental Figure 8. The *LYK3* Kinase-Inactive Mutant *hcl-1* Shows Altered Root Hair Morphology on Fåhraeus Medium.

Supplemental Figure 9. FLOT4:GFP Mislocalizes in Epidermal Cells of Mutants Carrying Mutations in Symbiotic Receptors.

Supplemental Figure 10. LYK3:GFP Complements the Decrease in FLOT4 Puncta Density in the *hcl-1* Mutant.

Supplemental Table 1. Transgenes Complement *lyk3* Mutant Symbiotic Phenotypes.

Supplemental Movie 1. Cytoplasmic LYK3:GFP Vesicles Are More pPrevalent after Bacterial Treatment.

Supplemental Movie 2. LYK3:GFP after Treatment with Buffer, *S. meliloti*, NF, and Bacterial Mutants Producing Altered NFs.

Supplemental Movie 3. LYK3:GFP and FLOT4:mCherry Distribution after Buffer Treatment.

Supplemental Movie 4. Positionally Stable LYK3:GFP and FLOT4:mCherry Puncta Colocalize after *S. meliloti* Treatment.

Supplemental Movie 5. FLOT4:mCherry Is Not Present on LYK3:GFP Vesicles after *S. meliloti* Treatment.

ACKNOWLEDGMENTS

We thank Q.D. Nguyen for construction of P_{trp}-*CFP* (pQDN01) and G. Grossmann, D. Bergmann, and our lab colleagues for helpful discussions. Financial support was provided by a National Science Foundation Graduate Research Fellowship award to C.H.H., by prior funds to S.R.L. from the Howard Hughes Medical Institute, and from the Hoover Circle Fund. Support to D.R.C. and B.K.R. was provided by Department of Energy Energy Biosciences Award DE-FG02-01ER15200. Support to D.W.E. was provided by National Science Foundation Award 0524334.

AUTHOR CONTRIBUTIONS

C.H.H., B.K.R., D.R.C., and S.R.L. designed the research. C.H.H. and B.K.R. performed research. D.M.T. contributed new experimental tools. C.H.H., S.R.L., and D.W.E. analyzed data, and C.H.H., S.R.L., D.W.E., B.K.R., and D.R.C. wrote the article.

Received April 23, 2011; revised June 7, 2011; accepted June 16, 2011; published July 8, 2011.

REFERENCES

Amor, B.B., Shaw, S.L., Oldroyd, G.E., Maillet, F., Penmetsa, R.V., Cook, D., Long, S.R., Dénarié, J., and Gough, C. (2003). The *NFP* locus of *Medicago truncatula* controls an early step of Nod Factor signal transduction upstream of a rapid calcium flux and root hair deformation. Plant J. **34:** 495–506.

Ané, J.M., et al. (2004). *Medicago truncatula DMI1* required for bacterial and fungal symbioses in legumes. Science **303:** 1364–1367.

Ardourel, M., Demont, N., Debellé, F., Maillet, F., de Billy, F., Promé, J.C., Dénarié, J., and Truchet, G. (1994). *Rhizobium meliloti* lipooligosaccharide Nodulation Factors: Different structural requirements for bacterial entry into target root hair cells and induction of plant symbiotic developmental responses. Plant Cell **6:** 1357–1374.

Ardourel, M., Lortet, G., Maillet, F., Roche, P., Truchet, G., Promé, J.C., and Rosenberg, C. (1995). In *Rhizobium meliloti*, the operon

associated with the nod box n5 comprises nodL, noeA and noeB, three host-range genes specifically required for the nodulation of particular *Medicago* species. Mol. Microbiol. **17:** 687–699.

Arrighi, J.F., et al. (2006). The *Medicago truncatula* lysin motif-receptor-like kinase gene family includes *NFP* and new nodule-expressed genes. Plant Physiol. **142:** 265–279.

Arrighi, J.F., Godfroy, O., de Billy, F., Saurat, O., Jauneau, A., and Gough, C. (2008). The *RPG* gene of *Medicago truncatula* controls *Rhizobium*-directed polar growth during infection. Proc. Natl. Acad. Sci. USA **105:** 9817–9822.

Boisson-Dernier, A., Chabaud, M., Garcia, F., Becard, G., Rosenberg, C., and Barker, D.G. (2001). *Agrobacterium rhizogenes*-transformed roots of *Medicago truncatula* for the study of nitrogen-fixing and endomycorrhizal symbiotic associations. Mol. Plant Microbe Interact. **14:** 695–700.

Catoira, R., Galera, C., de Billy, F., Penmetsa, R.V., Journet, E.P., Maillet, F., Rosenberg, C., Cook, D., Gough, C., and Dénarié, J. (2000). Four genes of *Medicago truncatula* controlling components of a Nod Factor transduction pathway. Plant Cell **12:** 1647–1666.

Catoira, R., Timmers, A.C., Maillet, F., Galera, C., Penmetsa, R.V., Cook, D., Dénarié, J., and Gough, C. (2001). The *HCL* gene of *Medicago truncatula* controls *Rhizobium*-induced root hair curling. Development **128:** 1507–1518.

Costes, S.V., Daelemans, D., Cho, E.H., Dobbin, Z., Pavlakis, G., and Lockett, S. (2004). Automatic and quantitative measurement of protein-protein colocalization in live cells. Biophys. J. **86:** 3993–4003.

Crane, C., Wright, E., Dixon, R.A., and Wang, Z.Y. (2006). Transgenic *Medicago truncatula* plants obtained from *Agrobacterium tumefaciens*-transformed roots and *Agrobacterium rhizogenes*-transformed hairy roots. Planta **223:** 1344–1354.

Curtis, M.D., and Grossniklaus, U. (2003). A gateway cloning vector set for high-throughput functional analysis of genes in planta. Plant Physiol. **133:** 462–469.

Davis, S.J., and Vierstra, R.D. (1998). Soluble, highly fluorescent variants of green fluorescent protein (GFP) for use in higher plants. Plant Mol. Biol. **36:** 521–528.

Demont, N., Debellé, F., Aurelle, H., Dénarié, J., and Promé, J.C. (1993). Role of the *Rhizobium meliloti nodF* and *nodE* genes in the biosynthesis of lipo-oligosaccharidic Nodulation Factors. J. Biol. Chem. **268:** 20134–20142.

Ehrhardt, D.W., Atkinson, E.M., Faull, K.F., Freedberg, D.I., Sutherlin, D.P., Armstrong, R., and Long, S.R. (1995). In vitro sulfotransferase activity of NodH, a nodulation protein of *Rhizobium meliloti* required for host-specific nodulation. J. Bacteriol. **177:** 6237–6245.

Ehrhardt, D.W., Atkinson, E.M., and Long, S.R. (1992). Depolarization of alfalfa root hair membrane potential by *Rhizobium meliloti* Nod Factors. Science **256:** 998–1000.

Ehrhardt, D.W., Wais, R., and Long, S.R. (1996). Calcium spiking in plant root hairs responding to *Rhizobium* nodulation signals. Cell **85:** 673–681.

Endre, G., Kereszt, A., Kevei, Z., Mihacea, S., Kaló, P., and Kiss, G.B. (2002). A receptor kinase gene regulating symbiotic nodule development. Nature **417:** 962–966.

Esseling, J.J., Lhuissier, F.G., and Emons, A.M. (2004). A nonsymbiotic root hair tip growth phenotype in NORK-mutated legumes: implications for nodulation factor-induced signaling and formation of a multifaceted root hair pocket for bacteria. Plant Cell **16:** 933–944.

Fisher, R.F., Egelhoff, T.T., Mulligan, J.T., and Long, S.R. (1988). Specific binding of proteins from Rhizobium meliloti cell-free extracts containing NodD to DNA sequences upstream of inducible nodulation genes. Genes Dev. **2:** 282–293.

Fisher, R.F., and Long, S.R. (1992). Rhizobium–plant signal exchange. Nature **357:** 655–660.

Gage, D.J. (2002). Analysis of infection thread development using Gfp- and DsRed-expressing *Sinorhizobium meliloti*. J. Bacteriol. **184:** 7042–7046.

Gutierrez, R., Lindeboom, J.J., Paredez, A.R., Emons, A.M., and Ehrhardt, D.W. (2009). Arabidopsis cortical microtubules position cellulose synthase delivery to the plasma membrane and interact with cellulose synthase trafficking compartments. Nat. Cell Biol. **11:** 797–806.

Haney, C.H., and Long, S.R. (2010). Plant flotillins are required for infection by nitrogen-fixing bacteria. Proc. Natl. Acad. Sci. USA **107:** 478–483.

Hirsch, S., Kim, J., Munoz, A., Heckmann, A.B., Downie, J.A., and Oldroyd, G.E. (2009). GRAS proteins form a DNA binding complex to induce gene expression during nodulation signaling in *Medicago truncatula*. Plant Cell **21:** 545–557.

Iizasa, E., Mitsutomi, M., and Nagano, Y. (2010). Direct binding of a plant LysM receptor-like kinase, LysM RLK1/CERK1, to chitin in vitro. J. Biol. Chem. **285:** 2996–3004.

Kaku, H., Nishizawa, Y., Ishii-Minami, N., Akimoto-Tomiyama, C., Dohmae, N., Takio, K., Minami, E., and Shibuya, N. (2006). Plant cells recognize chitin fragments for defense signaling through a plasma membrane receptor. Proc. Natl. Acad. Sci. USA **103:** 11086–11091.

Klaus-Heisen, D., Nurisso, A., Pietraszewska-Bogiel, A., Mbengue, M., Camut, S., Timmers, T., Pichereaux, C., Rossignol, M., Gadella, T.W., Imberty, A., Lefebvre, B., and Cullimore, J.V. (2011). Structure-function similarities between a plant receptor-like kinase and the human interleukin-1 receptor-associated kinase-4. J. Biol. Chem. **286:** 11202–11210.

Lefebvre, B., et al. (2010). A remorin protein interacts with symbiotic receptors and regulates bacterial infection. Proc. Natl. Acad. Sci. USA **107:** 2343–2348.

Levy, J., et al. (2004). A putative Ca^{2+} and calmodulin-dependent protein kinase required for bacterial and fungal symbioses. Science **303:** 1361–1364.

Limpens, E., Franken, C., Smit, P., Willemse, J., Bisseling, T., and Geurts, R. (2003). LysM domain receptor kinases regulating rhizobial Nod Factor-induced infection. Science **302:** 630–633.

Limpens, E., Mirabella, R., Fedorova, E., Franken, C., Franssen, H., Bisseling, T., and Geurts, R. (2005). Formation of organelle-like N_2-fixing symbiosomes in legume root nodules is controlled by *DMI2*. Proc. Natl. Acad. Sci. USA **102:** 10375–10380.

Marsh, J.F., Rakocevic, A., Mitra, R.M., Brocard, L., Sun, J., Eschstruth, A., Long, S.R., Schultze, M., Ratet, P., and Oldroyd, G.E. (2007). *Medicago truncatula NIN* is essential for rhizobial-independent nodule organogenesis induced by autoactive calcium/calmodulin-dependent protein kinase. Plant Physiol. **144:** 324–335.

Mbengue, M., Camut, S., de Carvalho-Niebel, F., Deslandes, L., Froidure, S., Klaus-Heisen, D., Moreau, S., Rivas, S., Timmers, T., Hervé, C., Cullimore, J., and Lefebvre, B. (2010). The *Medicago truncatula* E3 ubiquitin ligase PUB1 interacts with the LYK_3 symbiotic receptor and negatively regulates infection and nodulation. Plant Cell **22:** 3474–3488.

Meade, H.M., Long, S.R., Ruvkun, G.B., Brown, S.E., and Ausubel, F.M. (1982). Physical and genetic characterization of symbiotic and auxotrophic mutants of *Rhizobium meliloti* induced by transposon Tn5 mutagenesis. J. Bacteriol. **149:** 114–122.

Mitra, R.M., and Long, S.R. (2004). Plant and bacterial symbiotic mutants define three transcriptionally distinct stages in the development of the *Medicago truncatula*/*Sinorhizobium meliloti* symbiosis. Plant Physiol. **134:** 595–604.

Mitra, R.M., Shaw, S.L., and Long, S.R. (2004a). Six nonnodulating plant mutants defective for Nod Factor-induced transcriptional

changes associated with the legume-rhizobia symbiosis. Proc. Natl. Acad. Sci. USA **101:** 10217–10222.

Mitra, R.M., Gleason, C.A., Edwards, A., Hadfield, J., Downie, J.A., Oldroyd, G.E., and Long, S.R. (2004b). A Ca^{2+}/calmodulin-dependent protein kinase required for symbiotic nodule development: Gene identification by transcript-based cloning. Proc. Natl. Acad. Sci. USA **101:** 4701–4705.

Miyahara, A., Richens, J., Starker, C., Morieri, G., Smith, L., Long, S., Downie, J.A., and Oldroyd, G.E. (2010). Conservation in function of a SCAR/WAVE component during infection thread and root hair growth in *Medicago truncatula*. Mol. Plant Microbe Interact. **23:** 1553–1562.

Murray, J.D. (2011). Invasion by invitation: Rhizobial infection in legumes. Mol. Plant Microbe Interact. **24:** 631–639.

Oke, V., and Long, S.R. (1999). Bacterial genes induced within the nodule during the Rhizobium-legume symbiosis. Mol. Microbiol. **32:** 837–849.

Oldroyd, G.E., and Downie, J.A. (2008). Coordinating nodule morphogenesis with rhizobial infection in legumes. Annu. Rev. Plant Biol. **59:** 519–546.

Oldroyd, G.E., and Long, S.R. (2003). Identification and characterization of nodulation-signaling pathway 2, a gene of *Medicago truncatula* involved in Nod Factor signaling. Plant Physiol. **131:** 1027–1032.

Penmetsa, R.V., et al. (2008). The *Medicago truncatula* ortholog of Arabidopsis *EIN2*, *sickle*, is a negative regulator of symbiotic and pathogenic microbial associations. Plant J. **55:** 580–595.

Petutschnig, E.K., Jones, A.M., Serazetdinova, L., Lipka, U., and Lipka, V. (2010). The lysin motif receptor-like kinase (LysM-RLK) CERK1 is a major chitin-binding protein in Arabidopsis thaliana and subject to chitin-induced phosphorylation. J. Biol. Chem. **285:** 28902–28911.

Pitts, R.J., Cernac, A., and Estelle, M. (1998). Auxin and ethylene promote root hair elongation in Arabidopsis. Plant J. **16:** 553–560.

Quandt, H.J., Pühler, A., and Broer, I. (1993). Transgenic root nodules of *Vicia hirsuta*: A fast and efficient system for the study of gene expression in indeterminate-type nodules. Mol. Plant Microbe Interact. **6:** 699–706.

Riely, B.K., Lougnon, G., Ané, J.M., and Cook, D.R. (2007). The symbiotic ion channel homolog DMI1 is localized in the nuclear membrane of *Medicago truncatula* roots. Plant J. **49:** 208–216.

Robatzek, S., Chinchilla, D., and Boller, T. (2006). Ligand-induced endocytosis of the pattern recognition receptor FLS2 in Arabidopsis. Genes Dev. **20:** 537–542.

Roche, P., Debellé, F., Maillet, F., Lerouge, P., Faucher, C., Truchet, G., Dénarié, J., and Promé, J.C. (1991b). Molecular basis of symbiotic host specificity in *Rhizobium meliloti*: *nodH* and *nodPQ* genes encode the sulfation of lipo-oligosaccharide signals. Cell **67:** 1131–1143.

Roche, P., Lerouge, P., Ponthus, C., and Promé, J.C. (1991a). Structural determination of bacterial Nodulation Factors involved in the *Rhizobium meliloti*-alfalfa symbiosis. J. Biol. Chem. **266:** 10933–10940.

Salomon, S., and Robatzek, S. (2006). Induced endocytosis of the receptor kinase FLS2. Plant Signal. Behav. **1:** 293–295.

Schenk, R.U., and Hildebrandt, A.C. (1972). Medium and techniques for the induction and growth of monocotyledonous and dicotyledonous plant cell cultures. Can. J. Bot. **50:** 199–204.

Schultze, M., Staehelin, C., Röhrig, H., John, M., Schmidt, J., Kondorosi, E., Schell, J., and Kondorosi, A. (1995). In vitro sulfotransferase activity of *Rhizobium meliloti* NodH protein: lipochitooligosaccharide nodulation signals are sulfated after synthesis of the core structure. Proc. Natl. Acad. Sci. USA **92:** 2706–2709.

Shaw, S.L., and Long, S.R. (2003). Nod Factor elicits two separable calcium responses in *Medicago truncatula* root hair cells. Plant Physiol. **131:** 976–984.

Shearman, C.A., Rossen, L., Johnston, A.W., and Downie, J.A. (1986). The *Rhizobium leguminosarum* nodulation gene *nodF* encodes a polypeptide similar to acyl-carrier protein and is regulated by nodD plus a factor in pea root exudate. EMBO J. **5:** 647–652.

Smit, P., Limpens, E., Geurts, R., Fedorova, E., Dolgikh, E., Gough, C., and Bisseling, T. (2007). Medicago LYK3, an entry receptor in rhizobial nodulation factor signaling. Plant Physiol. **145:** 183–191.

Smit, P., Raedts, J., Portyanko, V., Debelle, F., Gough, C., Bisseling, T., and Geurts, R. (2005). NSP1 of the GRAS protein family is essential for rhizobial Nod factor-induced transcription. Science **308:** 1789–1791.

Swanson, J.A., Tu, J.K., Ogawa, J., Sanga, R., Fisher, R.F., and Long, S.R. (1987). Extended region of nodulation genes in *Rhizobium meliloti* 1021. I. Phenotypes of Tn5 insertion mutants. Genetics **117:** 181–189.

Szabados, L., Charrier, B., Kondorosi, A., de Bruijn, F.J., and Ratet, P. (1995). New plant promoter and enhancer testing vectors. Mol. Breed. **1:** 419–423.

Turner, G.L., and Gibson, A.H. (1980). Measurement of nitrogen fixation by indirect means. In Methods for Evaluation of Biological Nitrogen Fixation, F.J. Bergersen, ed (Chichester, UK: John Wiley & Sons), pp. 111–138.

Wais, R.J., Galera, C., Oldroyd, G., Catoira, R., Penmetsa, R.V., Cook, D., Gough, C., Dénarié, J., and Long, S.R. (2000). Genetic analysis of calcium spiking responses in nodulation mutants of *Medicago truncatula*. Proc. Natl. Acad. Sci. USA **97:** 13407–13412.

Wais, R.J., Keating, D.H., and Long, S.R. (2002). Structure-function analysis of Nod Factor-induced root hair calcium spiking in *Rhizobium*-legume symbiosis. Plant Physiol. **129:** 211–224.

Zacharias, D.A., Violin, J.D., Newton, A.C., and Tsien, R.Y. (2002). Partitioning of lipid-modified monomeric GFPs into membrane microdomains of live cells. Science **296:** 913–916.